RESULTS ON TOTAL AND ELASTIC CROSS SECTIONS IN PROTON-PROTON COLLISIONS AT $\sqrt{s} = 200$ GeV OBTAINED WITH THE STAR DETECTOR AT RHIC

B. Pawlik
Institute of Nuclear Physics PAN, Radzikowskiego 152,
31-342 Cracow, Poland

W. Guryn
Brookhaven National Laboratory, Department of Physics
Upton, NY 119735000, USA

We report the first results on differential, total and elastic cross sections in proton-proton collisions at the Relativistic Heavy Ion Collider (RHIC) at $\sqrt{s} = 200$ GeV. The data were obtained with the Roman Pot Detector subsystem of the STAR experiment. The data used for this analysis cover the four-momentum transfer squared (t) range $0.045 \geq -t \leq 0.135$ $(\mathrm{GeV/c})^2$. The Roman Pot system was placed downstream of the STAR detector. During the data taking the Roman Pots were moved to $8\sigma_y$, the vertical distance of from the beam center. They were operated during standard data taking procedure. The results include values of the exponential slope parameter (B), elastic cross section (σ_{el}) and the total cross section (σ_{tot}) obtained by extrapolation of the elastic differential cross section $(d\sigma/dt)$ to the optical point at $-t = 0$ $(\mathrm{GeV/c})^2$. The detector setup and analysis procedure are reviewed. All results are compared with the world data.

Presented at EDS Blois 2019
The 18th Conference on Elastic and Diffractive Scattering
Quy Nhon, Vietnam,
June 2328, 2019

1 The Experiment

Results presented here are based on data collected with pp2pp Roman Pots [1] part of the STAR detector [2] at RHIC. The Roman Pots (**RPs**) setup (Fig. 1) consisted of four stations with two of them (**W1,W2**) placed at ∼15.8 and ∼17.6 meters downstream, (West) from interaction point (**IP**) and other two (**E1,E2**) symmetrically upstream, (East) from **IP**. Each RP station consists of two Roman Pots (one above and the other below beam line) each equipped with package of 4 silicon strip detector (Si) planes, two planes for measuring X and the other two for Y positions of the particle track. The scintillation counter placed behind Si planes and read by two PMTs was used to trigger on candidate events. Candidate event had to fulfill the trigger condition, from here referred to as **RP_ET**, requiring presence of the signal in at least one Roman Pot (**RP**) on each side of **IP**.

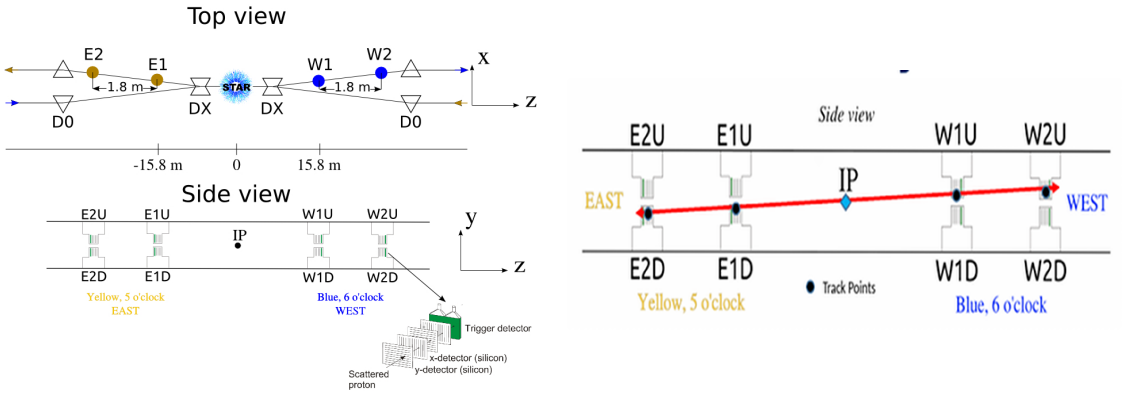

Figure 1 – The layout of Roman Pots system at STAR (left) and example of reconstructed points configuration for elastic event detected in arm EDWU (right) .

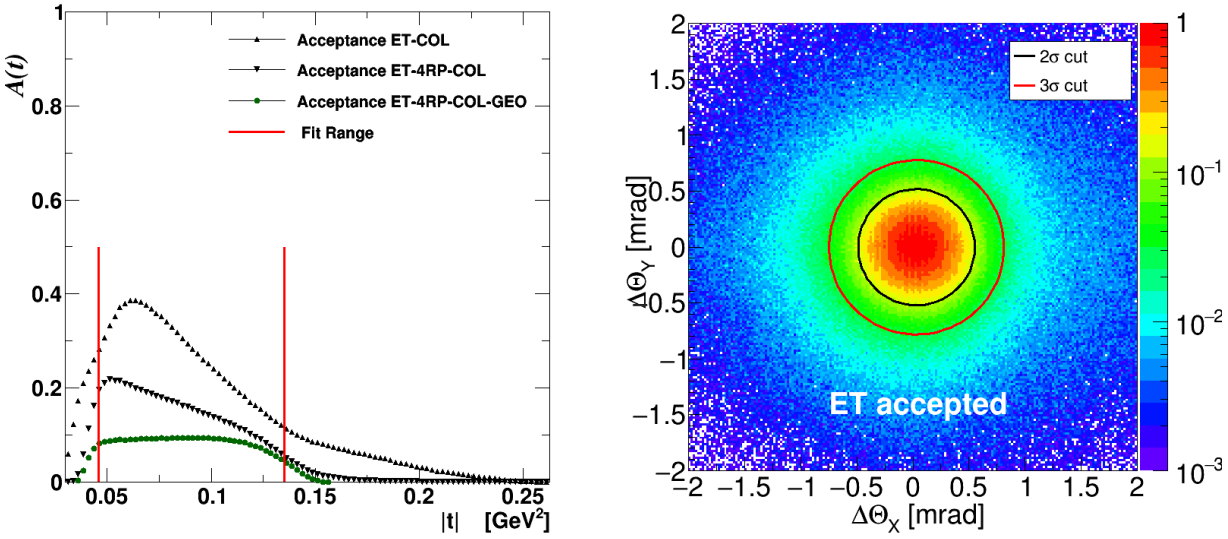

Figure 2 – Acceptance as function four-momentum transfer $\mathbf{t}$ (left), West-East co-linearity $\Delta\theta_Y$ vs $\Delta\theta_X$ (right).

2 Data Set

Data were taken with nominal beam conditions β^* =0.85 m, luminosity ≈45·10^{30} cm^{-2}sec^{-1}. There were approximately 6.7 millions events fulfilling trigger condition `RP_ET` recorded for integrated luminosity 1.8 pb^{-1}. The geometrical acceptance was constrained by the closest possible approach of the detector to the beam and, the aperture of the beam line elements (DX magnet) in front of the detector. The closest achieved distance of the first strip was ∼ 30 mm corresponding to minimum four-momentum transfer $|\mathbf{t}_{min}| \simeq 0.03$ GeV^2. The aperture of DX magnet sets the maximum achievable four-momentum transfer $|\mathbf{t_{max}}|$ ≈0.25 GeV^2. The detector acceptance as function of four-momentum transfer, $|\mathbf{t}|$, is shown in fig.2.

2.1 Event Reconstruction

All events collected with trigger `RP_ET` underwent reconstruction procedure. First, in all RPs in each detector Si plane clusters - continuous set of strips with signal above threshold - were formed. Next, clusters found in two X-planes were matched by comparing their positions x_1 and x_2 and finding the pair with minimum distance $\Delta x_c = |x_1 - x_2|$ smaller then 200 μm (twice Si detector strip pitch). Analogous procedure was repeated for two Y-planes. Unmatched clusters,

if any, were considered as detector noise or random background and were neglected. Pairs of clusters matched in x and y-plane defined space points X_{RP} and Y_{RP} coordinates of the proton track. These were used to calculate the local angles θ_x and θ_Y in (x,z) and (y,z) planes as:

$$\theta_X = \frac{X_{RP1} - X_{RP2}}{Z_{RP1} - Z_{RP2}} \quad and \quad \theta_Y = \frac{Y_{RP1} - Y_{RP2}}{Z_{RP1} - Z_{RP2}} \tag{1}$$

where subscripts RPs(RPs) denote RP stations 1(2) at same side of IP and $Z_{RP1}(Z_{RP2})$ are z-positions of the stations. For small scattering angles in this experiment, to a good approximation the four-momentum transfer, t, was calculated with formula:

$$t = -p^2 \cdot \theta^2 = -p^2 \cdot (\theta_X^2 + \theta_Y^2) \tag{2}$$

where p is proton momentum, $\theta = \sqrt{\theta_X^2 + \theta_Y^2}$ scattering angle and θ_X, θ_Y calculated as in Eq.1. The RPs system was positioned and aligned with respect to nominal beam trajectory, hence the angles θ_X and θ_Y provide direct measurement of the projections of scattering angle θ on (x,z) and (y,z) planes, respectively.

2.2 Elastic Scattering Event Selection

The hardware trigger requiring signal in at least one RP on each side of IP was very inclusive. The clean pattern indicating elastic scattering (see right subfigure in Fig.1) is presence of two back to back protons in the event. This requires signal only in top RP1 and/or RP2 at one side of IP and only in bottom RP1 and/or RP2 on the other side. Calculation of the track direction angles (Eq.1) requires points in two stations on the each side of IP.

The data sample used to obtain these results consist only of events with four reconstructed points (one point in each RP) , four points (**4PT**) events, and fulfilling West-East colinearity condition:

$$\Delta\theta = \sqrt{(\theta_X^{West} - \theta_X^{East})^2 + (\theta_Y^{West} - \theta_Y^{East})^2} < 2 \cdot \sigma_\theta \tag{3}$$

with $\sigma_\theta = 255$ μrad was dominated by the beam angular divergence ($\sim$ 180 μrad for each beam). The kinematic range of four-momentum transfer, **t**, versus azimuth angle ϕ for this sample (**4PT-COL**) is shown in Fig.3.

For the 4PT-COL events, scattering angles at the IP θ_X^*, θ_Y^* were obtained from the linear fit using four X_{RP} and Y_{RP} points. The four-momentum transfer, t, for those events was then calculated using Eq.2, where local angles θ_X, θ_Y were replaced respectively with θ_X^*, θ_Y^*.

Additionally, geometrical cut was imposed to reduce background by staying away from acceptance boundaries and maintain relatively flat, slow varying acceptance corrections (see data labeled as **ET-4RP-COL-GEO** in Fig.2). It was required that the scattered proton angles, θ and azimuth angle ϕ obey following limits:

$$79.5\,\texttt{[deg]} < |\phi| < 101.5\,\texttt{[deg]} \quad 2.0\,\texttt{[mrad]} < \theta < 4.0\,\texttt{[mrad]} \tag{4}$$

2.3 Monte Carlo Corrections

The beam line elements and all RP detectors were implemented in detail in Geant4[7] based Monte Carlo application. The events were generated according to standard formula for the elastic scattering differential cross section with the slope $B = 14.0$ GeV^{-2}, the parameter ρ=0.128 and West-Yennie[4] Coulomb phase. The beam angular divergence and the interaction point **IP** position uncertainty were included in the generator.

The experimental differential distributions dN/dt was corrected using "bin-by-bin" method with the formula:

$$\left(\frac{dN}{dt}\right)^{DATA}_{corrected} = \left(\frac{dN}{dt}\right)^{DATA}_{reconstructed} \times \frac{(dN/dt)^{MC}_{generated}}{(dN/dt)^{MC}_{reconstructed}} \tag{5}$$

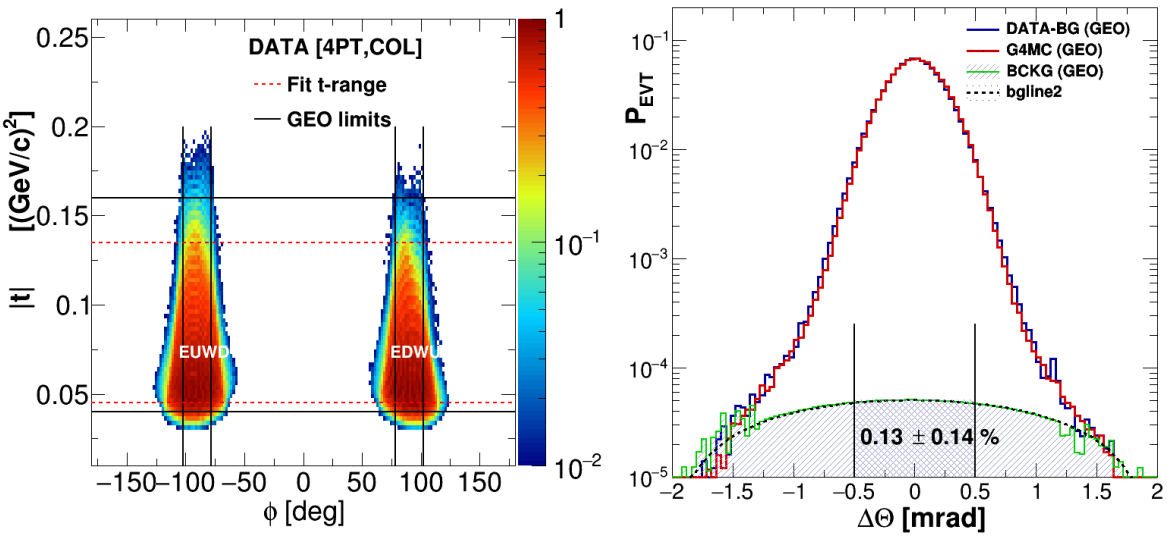

Figure 3 – Four-momentum transfer, $|t|$, vs azimuth angle, ϕ, for accepted ET colinear events with four reconstructed points (**4PT**) (left), and (right) background contribution estimate based on comparison of West-East colinearity $\Delta\theta$ for DATA and Monte-Carlo samples of **4PT** events within **GEO** limits (4).

where $(dN/dt)^{MC}_{generated}$ and $(dN/dt)^{MC}_{reconstructed}$ are true MC distribution and reconstructed based on MC event sample which passed the same reconstruction procedure and selection criteria as those applied for experimental data. The corrections obtained this way account for limited geometrical acceptance, effects of the scattering angle reconstruction resolution (**t**-smearing) and impact of the secondary scattering of the final state proton off the material on the way from **IP** to detector Si planes.

3 Results

The corrected differential cross section ($d\sigma/dt$) was fitted with standard formula[3,5,6]:

$$\frac{d\sigma_{el}}{dt} = \frac{1+\rho^2}{16\pi(\hbar c)^2} \cdot \sigma_{tot}^2 \cdot e^{-B|t|} \tag{6}$$

with ρ=0.128 from COMPETE [9] model. The Coulomb and interference terms were neglected as their contribution in the fit range $0.045 < -t < 0.135$ GeV^2 is negligibly small within this experiment's precision. The data and fit results are shown in Fig.4.

The total cross section, σ_{tot}, was calculated using the optical theorem as:

$$\sigma_{tot}^2 = \frac{16\pi(\hbar c)^2}{1+\rho^2} \cdot \frac{d\sigma_{el}}{dt}\Big|_{t=0} \tag{7}$$

and the total elastic cross section, σ_{el}, was obtained by integrating fitted formula (6) over whole t range, the elastic cross section integrated within the t-acceptance of this measurement (σ_{el}^{det}) is also quoted. The inelastic cross section is simply result of subtraction $\sigma_{inel}=\sigma_{tot} - \sigma_{el}$. All results with their statistical and systematic uncertainties are shown in Table 1.

4 Summary

The elastic differential cross section in pp scattering was measured with Roman Pots system of the STAR experiment at RHIC in t range $0.045 < -t < 0.135$ GeV^2 at $\sqrt{s}$=200 GeV. In this t range the cross section is well described by exponential $exp(-B \cdot t)$ with the slope B =

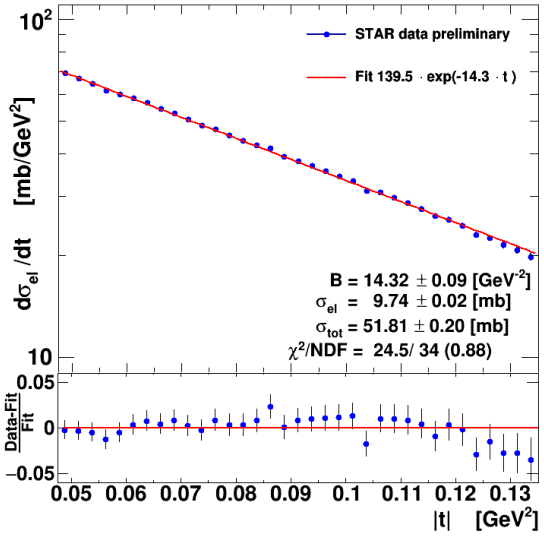

Figure 4 – Top panel: pp elastic differential cross-section, $d\sigma/dt$, fitted with exponential function $A \cdot exp(-Bt)$; Bottom panel: Residuals (Data - Fit)/Data.

Table 1: Results summary.

Quantity			Statistical	Systematic uncertainties			
name	units	Value	uncertainty	beam-tilt	luminosity	ρ	full
$d\sigma_{el}/dt\|_{t=0}$	[mb/GeV^2]	139.53	$\pm$1.06	$^{+1.07}_{-0.83}$	$^{+10.50}_{-10.07}$	n/a	$^{+10.55}_{-10.10}$
B	[GeV^{-2}]	14.32	$\pm$0.09	$^{+0.18}_{-0.32}$	n/a	n/a	$^{+0.18}_{-0.32}$
σ_{el}	[mb]	9.74	$\pm$0.02	$^{+0.06}_{-0.04}$	$^{+0.74}_{-0.59}$	n/a	$^{+0.74}_{-0.59}$
σ_{el}^{det}	[mb]	3.63	$\pm$0.01	$^{+0.02}_{-0.01}$	$^{+0.28}_{-0.23}$	n/a	$^{+0.28}_{-0.23}$
σ_{tot}	[mb]	51.81	$\pm$0.20	$^{+0.19}_{-0.61}$	$^{+1.91}_{-1.90}$	$^{+0.20}_{-0.40}$	$^{+1.93}_{-2.04}$
σ_{inel}	[mb]	42.07	$\pm$0.20	$^{+0.20}_{-0.61}$	$^{+2.05}_{-1.99}$	$^{+0.20}_{-0.40}$	$^{+2.07}_{-2.12}$

$14.32\pm0.09(^{+0.18}_{-0.32})$ GeV^{-2}, in brackets full systematic errors are given. The elastic cross section integrated within detector acceptance $\sigma_{el}^{det} = 3.63\pm0.01(^{+0.28}_{-0.23})$ mb, extrapolation of this measured cross section over undetected (60%) t region results in value of the total elastic cross section σ_{el}=$9.74\pm0.02(^{+0.74}_{-0.59})$ mb. Using optical theorem we found the value of total pp scattering cross section σ_{tot}=$51.81\pm0.20(^{+1.93}_{-2.04})$ mb.

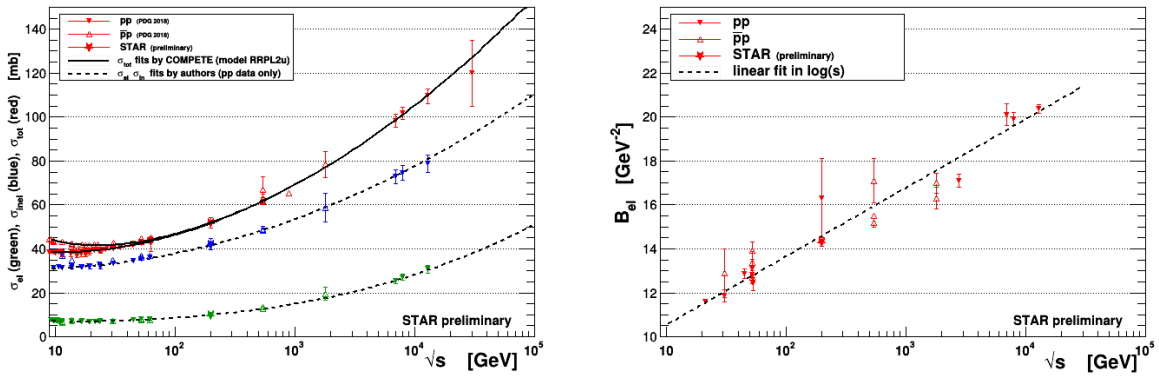

Figure 5 – Comparison of the STAR result on $\sigma_{tot}, \sigma_{el}$ and σ_{inel} (left) and B-slope (right) with the world data on cross sections [8] and B-slopes [11,12,13,14,16,17,19,20], COMPETE prediction [9] for σ_{tot} and σ_{inel} are displayed.

The results obtained with STAR are compared with the world data in Fig.5. We found they compare well and follow COMPETE prediction of dependence of cross section on $\sqrt{s}$.

Acknowledgments

This work was partly supported by the National Science Center of Poland under grant number UMO-2015/18/M/ST2/00162.

References

1. S. Bultmann *et al.*, *Nucl. Instrum. Methods* **535**, 415 (2004).
2. visit https://www.star.bnl.gov
3. B. Z. Kopeliovich, I. K. Potashnikova and B. Povh, Phys. Rev. D **86**, 051502 (2012) [arXiv:1208.5446 [hep-ph]].
4. Geofrey B. West and D.R. Yennie, Phys. Rev.**172**,1413.
5. V. Barone, E. Predazzi, *High-Energy Particle Diffraction*, Texts and Monographs in Physics, Springer-Verlag; (2002), ISBN: 3540421076.
6. S. Donnachie, G. Dosch, P. Landshoff, *Pomeron Physics and QCD*; Cambridge University Press; (1998), ISBN: 9780521675703.
7. S. Agostinelli *et al.*, Nucl. Instrum. Meth. A 506 (2003) 250-303.
   or visit http://geant4.web.cern.ch/geant4
8. M. Tanabashi *et al.*, (Particle Data Group), Phys. Rev. **D98**, 030001 (2018), http://pdg.lbl.gov/2018/hadronic-xsections/hadron.html
9. J. R. Cudell, *et al.*, (COMPETE Collaboration), Phys. Rev. Lett. **89** (2002) 201801.
10. U. Amaldi *et al.* (CERN-Pisa-Rome-Stony Brook Collaboration), Phys. Lett. **62B**, 460 (1976).
    U. Amaldi *et al.*, Phys. Lett. B43, 231 (1973).
11. G. Barbiellini *et al.*, Phys. Lett. **39B**, 663 (1972).
12. M. Ambrosio *et al.*, Phys. Lett. **115B**, 495 (1982).
13. N. A. Amos *et al.*, Phys. Lett. **120B**, 460 (1983).
14. S. L. Bueltmann *et al.*, Phys. Lett. B **579**, 245 (2004)

15. G. Antchev *et al.* (TOTEM Collaboration), Nucl. Phys. B **899**, 527 (2015)
16. G. Antchev *et al.* (TOTEM Collaboration), Eur. Phys. J. C **79**, no. 2, 103 (2019) and references therein
17. G. Antchev *et al.* (TOTEM collaboration), *Phys. Rev. Lett.* **111** no. 1, (2013) 0112001.
18. G. Antchev *et al.*, (TOTEM collaboration), *EPL* **101** no. 2, (2013) 21002.
19. G. Aad *et al.*(ATLAS collaboration), Nucl. Phys. **B889** (2014) 486.
20. M. Aaboud *et al.*, (ATLAS collaboration), Phys. Lett. *B761* (2016) 158.